International Journal of Mechanical And Production Engineering, ISSN: 2320-2092, Volume- 5, Issue-9, Sep.-2017
http://iraj.in

DESIGN AND SIMULATION OF AN OPPOSED-PISTON ENGINE WORKED BY THE RESONANT AND FOCUSING OF THE SHOCK WAVE

[1]CHANG-HSIEN TAI, [2]UZU-KUEI HSU, [3]CHING-CHANG LAI

[1,3]Dept. of Vehicle Engineering, National Pingtung University of Sci. & Tech., Taiwan, ROC
[2*]Dept. of Aircraft Engineering, Air Force Institute of Technology, Taiwan, ROC
E-mail: ukhsu@ms48.hinet.net

Abstract- This paper was carried out a design to produce high-pressure shock-wave forms in order to increase the efficiency of the energy concentrated by the shock reflection, resonant or focusing. In this study, numerical simulation was adopted to analyze the interaction between shock waves and moving boundaries. The CFD method is applied to simulate the shock resonant or focusing in an opposed-piston engine driven by shock wave. The finite volume method for solving Navier-Stokes equations to investigate the resonant and focusing of the shock wave in a typical cylinder. The test parameters are including of pressure source, temperature, piston weight and high-pressure release time. This analysis allowed for the identification of the interdependence among the parameters involved when shock waves are used to concentrate energy. The results of this study provide a reference for follow-up experiments and future system design of a magnetic-fluid generator.

Indexterms- Shock wave, Opposed-piston engine, Resonant, Focusing, CFD.

I. INTRODUCTION

Presently, solar, wind, geothermal, hydro, tidal, ocean thermal energy conversion, and biomass technologiesare the most feasible renewable energy sources [1]. The consistent collection of renewable energy and economic benefits of these technologiesare typically hindered by a variety of factors, such as climate, location, and equipment size, all of which require improvement.Recently, power grids that integrate solar and wind energy have concurrently been developed (e.g., at the National Renewable Energy Laboratory, US Department of Energy [2]). Additionally, research institutions in Taiwan are promoting the development and designof power infrastructure systems that integrate multiple renewable energy sources. In Taiwan, mainstream renewable energy development has focused on wind and solar power. Wind power is limited by insufficient regional space in Taiwan, necessitating offshore development. Moreover,photovoltaics were initially implemented by the Taiwan Power Company by using large-scale systems, and other novel renewable energies, such as geothermal and ocean power, have yet to reach technological maturity.

Shortening energy conversion pathways optimizes conversion efficiency. To achieve this, various types of energy conversion technology are commonly applied, particularlypumped-storage hydroelectricity, which currently has the highest capacity of all energy storage methods. This method involves applying excess power to pump water into reservoirs, using difference in the water level to convert fluid energy into mechanical energy, thereby generating power. Despite the maturity of relevant technology, pumped-storage hydroelectricityis typically constrained by environmental factors. Additionally, automotive internal combustion engines convert chemical energy to mechanical energy, which can then be used to power automobiles and generate electric power through the electric generator before being subjected to chemical reaction and directed toward the storage battery. Current fluid-based energy storage technology stores high-pressure compressed air more easily than it does for thermal energy. At a volume identical to that of thermal energy, high-pressure compressed air can be stored at a high energy density. Compared with thermal energy, high-pressure compressed air is less susceptible to storage loss and has fewer restrictions on storage volume, rendering it effective for short-term energy storage. Recently, compressed air energy has also gained broad acceptance in the automotive industry because of its low energy consumption, lack of pollution, and minimal maintenance costs.

Currently, compressed air can be obtained at a low cost through renewable energy, such as wind power. Wind energy can be harnessed to directly compress air and prevent energy loss through other segments of conversion. Alternatively, excess off-peak electricity can be used to power air compressors, thereby storing compressed air in high-pressure storage tanks as energy relay stations. Compressed air is typically used to generate electricity by driving turbines. By contrast, in this study, shock waves generated during the sudden release of compressed air were harnessed to facilitate resonant movements. Shock waves travel at highspeeds. Theoretically, rapid shock-wave movement renders electricity generation through magnetic particle resonation highly feasible.

Since Emst Mach[3] first discovered the seismic reflection phenomenon in 1878, numerous studies have been performed to examine this phenomenon. Studies on shock-wave behavior have analyzed interactions at various boundaries (i.e., solid and free boundaries) between sets of shock waves or between

shock waves and boundary layers. Additionally, the diffraction phenomenon, which occurs when shock waves travel through the cross section of a sudden expansion, has also been analyzed[4].Shock waves can be applied to a wide range of studies, including studies related to healthcare, industry, and disaster forecasts. The physical phenomena of shock waves have been studied for many years, and researchers have adopted numerical methods for predicting the results of shock waves. Shock waves have been examined by researchers in various fields, including aerospace engineering, material processing and manufacturing, biology, military explosive design, internal combustion engine design, exhaust system design, microelectronics, and healthcare (i.e., lithotripsy [5]).

Assume that shock wavesare a one-dimensional inviscid flow. A shock-wave movement is theoretically accompanied by the formation of three wave types: compression waves, expansion waves, and contact waves. Compression waves travel faster than contact waves do; therefore,discussions on shock-wave phenomena are typically concentrated on compression waves. However, when applying shock waves in an enclosed space, the seismic reflections off the walls, intrinsic reflections of the compression waves, and subsequently formed shock waves must be considered. The interaction between the three types of waves (specifically the unsteady shock waves) and obstruction surface (particularly the moving boundary) has seldom been investigated. At the moment of blast, high-temperature and high-pressure shock waves are formed, disseminating outward. Subsequently, an overpressure forms when shock waves continue to spread to a certain point in space, exceeding the ambient pressure. During this process, the impact stress generated by the air particles along high-speed shock-wave movements is called dynamic pressure [6, 7]. During a blast, a fixed object becomes compressed. In this event, the shock-wave transmission process comprises three periods. As compression waves contact an object, the initial atmospheric pressure rapidly increases to a maximum, called the peak overpressure. The duration of the overpressure is called the positive duration. As shock waves spread outward, air surrounding the initial position of the blast is removed, reducing the surrounding pressure below the atmospheric pressure. This low-pressure zone subsequently draws surrounding air toward the point of blast, restoring atmospheric pressure. In a blast, shock waves expand outward in a high-speed and high-pressure spherical gaseous entity. This entity damages objects on impact, causing two main effects. One effect is the instantaneous highimpact of the overpressure on objects, which damages objects.The dynamic pressurecanmove objects and thus damage them on impact. The detonation impact of shock waves is closely related to distance from the explosion (increasing distance weakens detonation impact), and increasing overpressure magnifies the impact of shock waves on people and objects.

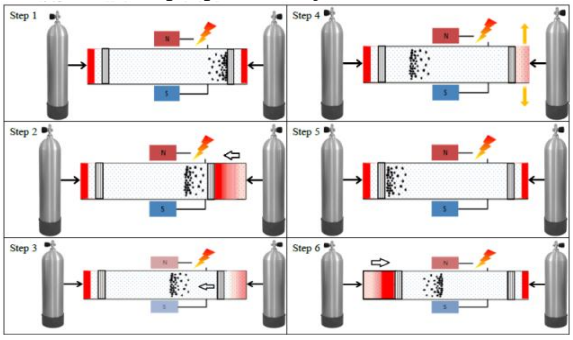

Flow chart of a typical opposed-piston engine driven by shock wave, ex: MHD generator.

Figure 1. Initial pressure distribution in the two-way shock tube

II. PHYSICS PROBLEM DESCRIPTION

In this study, a shock tube was applied to investigate the flow field effects and properties generated when shock waves impinge on a pair of pistons and to examine changes in physical properties within the tube under various operating conditions. This process combined the shock waves generated from the high-pressure source in the mid-section of the shock tube. Seismic resonances must be generated through the continuously coordinated motions of the pistons and high-pressure source to stabilize shock wave combination because persistency and stability are critical in the study of seismic resonances.

A space in the initial setting comprised high-pressure and low-pressure zones as well as a piston at each end in the numerical simulation (figure 1). The purpose of this setting was to facilitate investigating the mass flow rates (MFRs) of resonant pressures when observed under various conditions and variables. A diaphragm divided the high-pressure and low-pressure interfaces. When the diaphragm opened, the surface of the high-pressure gas formed a planar shock wave, propagating toward the low-pressure zone. When shock waves impinge on a piston (i.e., begin to impinge on the left piston), the movement compresses the gas in the opposite compression chamber, forming secondary shock waves. This shock wave continues propagating forward to the right piston, compressing the space between the right piston and high-pressure gas. The seismic reflections immediately return the piston to the left side. This response returns the piston past its original position, generating a negative pressure. Subsequently, the high-pressure source on the right side can be activated in a timely manner, impinging on the right

piston to generate shock waves. The newly produced shock wave travels faster than the reflected wave, approaching the speed of the preceding seismic reflection. When the generated shock wave and reflected wave from the right piston combine, the resultant shock wave is called seismic resonance. In this study, the combination of shock waves at the center of the shock tube was observed and investigated. The MFRs at the center of the shock tube were observed, and maximum resonance was maintained; these results can serve as a reference for future research involving the seismic resonance of magnetic fluids.

III. MATHEMATICAL MODEL

A. Basic Assumptions

The basic assumptions for the relevant fluid-body parameters were adopted to facilitate subsequent numerical simulations:

1) compressible flow
2) inviscid fluid
3) ideal gas
4) adiabatic walls

B. Governing Equations

When the shock waves interact with themovable solid walls at the two sides of the tube, the shock waves within the shock tube exhibit supersonic states. In this study, the time-dependent Reynolds-averaged Navier–Stokes equations were thus adopted in the mathematical model. However, to facilitate the use of the model in various flow-field calculations, data were calculated in discrete physical space by using the finite volume method. When combined with compressible flow and explicit time approximation, the space and time terms in the integrated governing equations (shown in the following equation) were separately processed.

$$\frac{\partial}{\partial t}\iiint_{\Omega} U d\Omega + \iint_{S} \vec{\Phi}\cdot d\vec{S} = 0 \quad (1)$$

$$\mathbf{U} = \begin{bmatrix} \rho \\ \rho u \\ \rho v \\ \rho w \\ \rho E \end{bmatrix} \quad \mathbf{F} = \begin{bmatrix} \rho u \\ \rho u^2 + p - \tau_{xx} \\ \rho uv - \tau_{xy} \\ \rho uw - \tau_{xz} \\ \rho u H^* - u\tau_{xx} - v\tau_{xy} - w\tau_{xz} + q_x \end{bmatrix}$$

$$\mathbf{G} = \begin{bmatrix} \rho v \\ \rho uv - \tau_{xy} \\ \rho v^2 + p - \tau_{yy} \\ \rho vw - \tau_{yz} \\ \rho v H^* - u\tau_{xy} - v\tau_{yy} - v\tau_{yz} + q_y \end{bmatrix} \quad (2)$$

$$\mathbf{H} = \begin{bmatrix} \rho w \\ \rho uw - \tau_{xz} \\ \rho vw - \tau_{yz} \\ \rho w^2 + p - \tau_{zz} \\ \rho w H^* - u\tau_{xz} - v\tau_{yz} - w\tau_{zz} + q_z \end{bmatrix}$$

C. Boundary conditions

Two-way shock waves were used in this study to impinge on the two opposing pistons. The movement involved controlling pressure activation and release mechanisms. The high-pressure sources were located at opposite ends of the device (figure 1). The horizontal and vertical boundaries of the high-pressure sources were configured as the pressure outlets. A diaphragm was placed on the boundary (dotted line) of the high-pressure source (facing the shock tube) to separate the high- and low-pressure gases. This boundary setting was timely adjusted to the wall boundary according to the mechanistic movements. The dashed circle indicates the moving wall; the boundaries represent the wall configurations; and the left and right sides of the shock wave tube also had identical settings. The center of the shock tube interior consisted of a detection line for recording and determining the conditions and numerical values of shock wave combinations.

IV. NUMERICAL METHOD AND GRID SYSTEM

A. Grid system

In this study, a shock tube comprising two opposing pistons, driven by shock waves generated using a high-pressure source, was adopted as the experimental model. The flow field properties and physical phenomena of the seismic resonance generated on the back-pressure side of the pistons, particularly during the shock wave combination and resonance processes, were used to investigate the shock wave–piston interaction. Suitable grid density is crucial for calculating numerical data and obtaining accurate results. All grids were generated using the H-Type and adaptive grid methods. Additionally, this study adopted Roberts'[8] sparsity transformation method to calculate the thickness of the first grid layer (y^+=0.2) and total number of grids (98,765).

B. Numerical method

This study used the finite volume method [9], [10] as the main numerical method for applying integrated time-dependent governing equations to calculate each grid in the model based on discrete time and space terms. First, afirst-order upwind scheme, thevan Leer Kappa Scheme (k=1/3)[11], and interpolation methods were adopted to calculate fluid-body variables near the two sides of the grid interfaces. The inviscid flux in the main equations (continuity, momentum, and energy equations) were calculated using Roe's Scheme[12], whereas the turbulent kinetic energy and convective flux of the dissipation transport equations were processed using the Jameson Scheme [9]. Additionally, viscous and diffusive fluxes were calculated using the central differencing scheme. Discretizing the space terms yielded a set of ordinary differential equations, which were

subsequently solved through time approximation or integration. To accelerate program convergence and enhance process stability, explicit and implicit residual smoothing, local time-stepping[9], and optimal explicit multistage scheme smoothing[13], [14] were adopted for time integrationto accelerate convergence into steady-state solutions.

V. RESULTS AND DISCUSSION

A. Defining the Release Timing

After the high-pressure release valves were activated, the shock waves impinged on the piston wall. The shock-wave energy propelled the piston until a peak pressure appeared at the other end of the piston. The transmission times of the reflected wave in the high-pressure zone were then observed using the mid-time point,at which the reflected wave impinges on the piston for the second time, as the pressure release time (figure2). The first derived time point was adopted in the initial release mechanism and all subsequent valve release operations. Two separate cases were used to determine the optimal valve release mechanism: In Case 1, an identical valve mechanism was adopted for the other piston without redetermining the activation timing, whereas in Case 2, the activation timing was separately determined for each piston.

The results showed that the MFR in Case 2 substantially exceeded that in Case 1 because of considerable energy loss, which was attributable to the lack of fixed timing for valve release and closure in Case 1 (figure3). Therefore, the stability of resonant movement and quality of the detected data were assessed, and the Case 2 results were found to be favorable. Therefore, the Case 2 mechanism was adopted for subsequent parameter changes.

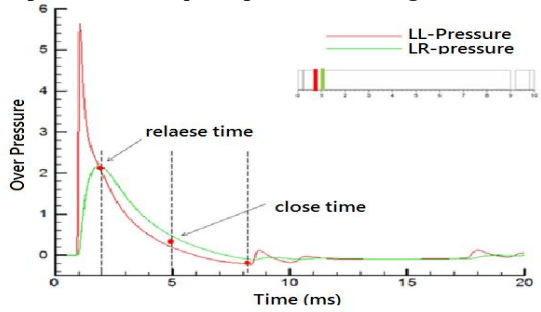

Figure. 2. Pressures on the left wall and corresponding release time points.

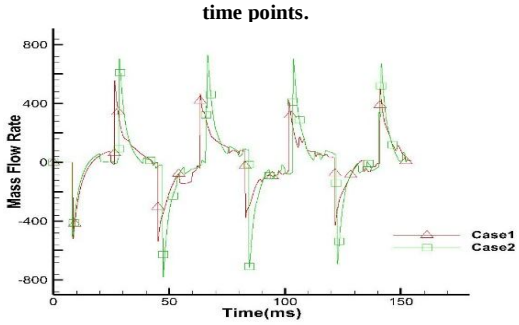

Figure. 3. MFRs in Cases 1 and 2.

C. Influence of Piston Weight

Based on the test results, an optimal actuation mode was determined. This mode featured the initial conditions, comprising a 10-atm high-pressure source, 500-K source temperature, and 0.5-kg piston mass. Piston mass was first assessed to optimize simulation cases for each parameter andinvestigate whether seismic resonance properties vary when continuous shock waves impinge on pistons of varying masses through a number of resonant interactions. Theoretically, the mass of moving components (pistons) in a mechanical device at fixed operating pressures is inversely related to the energy efficiency of the overall persistent resonant movement. Light pistons supposedly save energy and enhance the shock-wave intensities resulting from piston impingements. In this study,the experimental cases comprised the four piston masses of 0.1, 0.5, 1.0, and 2.0kg. Seven resonance tests were conducted after the first high-pressure seismic resonance (not counted) to establish clear relationships between pressure and piston mass (figure4 and 5). When the piston mass was 0.1kg, the resonant process demonstrated efficiency superior to that of all other piston masses. When pistons were heavy, the resonant data during each resonant session were substantially lower than those produced when light pistons wereused, suggesting that insufficient thrust and piston inertia prevented the shock-wave energy from maintaining stable shock-wave combinations. After the sixth resonant operation, the measured pressures and MFRs began to destabilize, demonstrating interference with other reflected waves. The combined shock-wave energy became increasingly dispersed, generating stochastic data. Moreover, the results also clearly demonstrated prolonged resonant time for the heavy pistons (figure6). The results yielded a best-case scenario that comprised a 10-atm source pressure and 0.1-kg piston mass and that is based on the assessment of resonant intervals. For example, the valve activation times for a 0.1-kg piston no longer decreased after the fourth resonance and began to demonstrate stable activation intervalsin which high-pressure air is activated once every 19 ms.

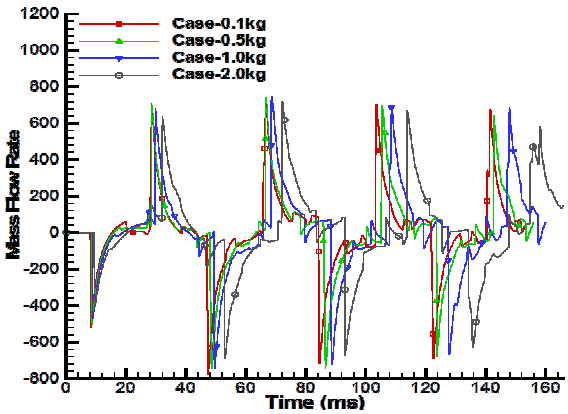

Figure4. Resonant MFRs for various piston masses.

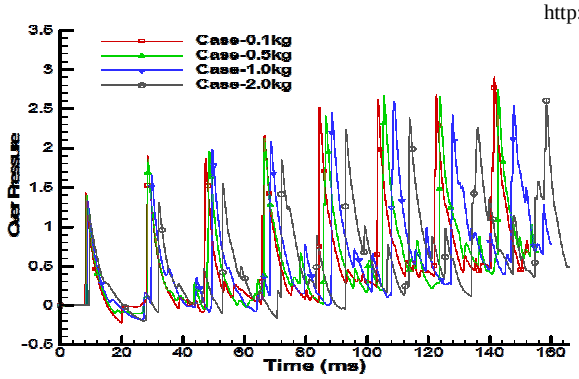

Figure5. Resonant pressures for various piston masses.

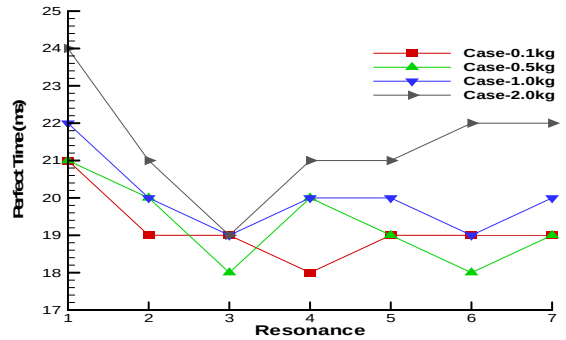

Figure6. Resonant time intervals for various piston masses.

Table 1
Relationship between pressure and mass flow rate

Pressure (atm)	Mass Flow rate Avg. (kg/s)	MFR Multiple
5	382	1 (base)
10	730	1.9
15	986	2.58
20	1198	3.13

CONCLUSION

1) In the example of the two-way resonant opposed-piston engine, the first impingement yielded the lowestMFRs.The impingements thereafter reduced the variations in the peak MFR at the center of the shock tube. Varying piston masses showed minimal differences among the average MFRs.The time required to reach stability in the resonant movements facilitated parameter optimization for the resonant shock tube.

2) When piston masses varied at constant working pressures, heavy pistons yielded inferior resonant efficiency compared with other pistons, and maintaining the stability of resonant MFRs and pressure was difficult because of seismic reflection.

3) The resonant MFRs exhibited maximum variations of 2.7% when the temperature was varied between 300 and 500 K. When piston masses ranging between 0.1 and 0.5 kg were used, MFRs varied by 1.4% and 2.3% at a working pressure of 10 and 15 atm, respectively. These parameter tests showed that the MFRs were primarily determined by the varying pressure sources.

REFERENCES

[1] Hsu, H.H., Chou, C., Wu, Y.C., Lu, M.M., Chen, C.T., Chen, Y.M., “Climate Change in Taiwan: Scientific Report 2011 (Summary),” National Science Council, Taipei, Taiwan, ROC, 2011.

[2] National Renewable Energy Laboratory, “Energy Management and Grid SupportApplications,”, December6, 2011.

[3] Mach, E., “Uber den Verlauf vonFunkenwellen in der Ebene und im Raume,” Sitzumgsher. Akad. Wiss. Wien. 78, pp. 819-838, 1878.

[4] Izumi, K., Aso, S. and Nishida, M., “Experimental and computational studies focusing processes of shock waves reflected from parabolic reflectors Shock Waves, Vol. 03, pp. 213-222, 1994.

[5] Jagadeesh, G., “Industrial applications of shock waves,” Proc. IMechE, Vol. 222, Part G: J. Aerospace Engineering, pp. 575–583, 2008.

[6] Montgomery, H., and J. Ward., “FacilityDamage and Personnel Injurt from Explosive Blast,”Designer’s Notebook. pp. 8-12, 1993.

[7] Ngo, T., Mendis, P., Gupta A., and Ramsay, J., “BlastLoading and Blast Effects on Structures – An Overview,” The University of Melbourne, Australia, 2007.

[8] Tannehill, J.C., Anderson, D.A. and Pletcher, R. H., “Computational Fluid Mechanics and Heat Transfer”, Taylor & Francis Group, pp.333-338, 1997.

[9] Jameson, A., Schmidt, W., and Turkel, E., "Numerical Solutions of the Euler Equations by a Finite Volume Method Using Runge-Kutta Time-stepping Schemes," AIAA Paper 81-1259, 1981.

[10] Hirsch, C.,"Numerical Computation of Internal and External flow”, Vol. 1, John Wiley & Sons Ltd., ch.6, 1989.

[11] van Leer. B., " Upwind-Difference Methods for Aerodynamic Problems Governed by the Euler Equations, in Large-Scale Computations in Fluid Mechanics," Lectures in Applied Mathematics, Vol. 22, pp. 327-336, 1985.

[12] Roe, P. L., "Approximate Riemann Solvers, Parameter Vector, and Difference Schemes," Journal of Computational Physics, Vol. 43, pp.357-372, 1981.

[13] Tai, C. H., Sheu, J. H. and van Leer B., “Optimal Coefficients of Multistage Schemes for the Euler Equations with Residual Smoothing,” AIAA Journal., Vol.33, No.6, pp.1008-1016, 1995.

[14] Tai, C. H., Sheu, J. H. and Tzeng, P. Y., “Improvement of Explicit Multistage Schemes for Central Spatial Differencing,” AIAA Journal., Vol. 34, No. 1, pp.185-188, 1996.

★★★